Dynamic Imaging Reveals Coordinate Effects of Cyclic Stretch and Substrate Stiffness on Endothelial Integrity

Arkaprava Dan,[1] Ryan B. Huang,[1] and Deborah E. Leckband[1,2]

[1]Department of Chemical and Biomolecular Engineering, University of Illinois, 600 South Mathews Avenue, Urbana, IL 61801, USA; and [2]Department of Chemistry, University of Illinois, 600 South Mathews Avenue, Urbana, IL 61801, USA

Associate Editor Konstantinos Konstantopoulos oversaw the review of this article.

Abstract—We describe an equibiaxial cell stretcher and hybrid, elastic membrane platform designed for dynamic imaging of cells on substrates with physiological stiffness undergoing cyclic stretch. Studies enabled by this device revealed that both substrate stiffness and cyclic stretch coordinately protect pulmonary endothelial monolayers against thrombin-induced disruption. The fluorescence imaging possible with the designed hybrid membranes further revealed similarities and differences in actin and cell dynamics during monolayer recovery. The improved live-cell imaging capabilities of this platform, when used in conjunction with fluorescent probes, will have broad applications for investigations of the impact of biochemical stimuli and mechanotransduction mechanisms on mechanically perturbed tissues.

INTRODUCTION

A range of mechanical cues influence vascular endothelial function, including fluid shear stress, hydrodynamic pressure and tissue stiffness.[9] The pulmonary endothelium may also experience cyclic equibiaxial strain during respiration.[26] The pulmonary endothelium is critical to maintaining the blood-gas barrier, and endogenous and exogenous mechanical stimuli can disrupt force balances postulated to maintain endothelial homeostasis.[8] Large-amplitude pathological cyclic strain (CS) has been shown to delay barrier recovery after treatment with inflammatory mediators like thrombin, whereas physiological CS protects against barrier failure.[2–4]

In addition to cyclic strain, tissue stiffness also influences endothelial permeability.[12,17] The physiological relevance of these observations is supported by *in vivo* studies demonstrating the increased permeability of stiffer, aged arteries[12] and increased vascular permeability in fibrotic lungs.[14,17] Such observations strongly suggest that mechanotransduction signals play an important role in endothelial barrier regulation, and further suggest links between vascular stiffness and disease. However, the underlying mechanisms, their response to altered stimuli such as cyclic strain and matrix rigidity, and their broader impact on endothelial barrier properties have yet to be established. Limitations in current experimental approaches present challenges to addressing these questions.

To mimic the mechanical environments of some tissues such as the lung, some *in vitro* approaches enable cell monolayer stretching, using substrates of physiologically relevant stiffness.[7,20,23,25] Common strategies for generating substrate strain involve membrane deformation techniques, such as use of positive or negative pressure, or indentation by non-flat or non-circular indenters. The latter approaches can impede dynamic cell imaging, because they move the cell monolayer out of the focal plane. These approaches also generate spatially non-uniform strain fields.[22] Alternative configurations generate uniform equibiaxial strain across a horizontal circular membrane, and avoid focal plane changes during stretch, by stretching membranes over flat cylindrical posts or drums.

Dynamic visualization of subcellular changes during continuous stretching is also a challenge. Elastic silicone membranes are conventionally used due to their bio-

Address correspondence to Deborah E. Leckband, Department of Chemical and Biomolecular Engineering, University of Illinois, 600 South Mathews Avenue, Urbana, IL 61801, USA. Electronic mail: leckband@illinois.edu

compatibility, optical properties, and ease of use. However, not all stretching configurations permit live-cell imaging. Silicone materials, and thicknesses required for mechanical durability, can increase background fluorescence and limit resolution, thus requiring cell fixation. For example, commonly used durable, thick (~0.20–0.25 mm) commercial silicone sheeting,[2,10,23,26] is translucent rather than transparent, and autofluorescence. Alternatively, polydimethylsiloxane (PDMS) membranes have superior optical properties, low autofluorescence, and can be cast in custom dimensions.[7,20] However, casting durable PDMS membranes requires compromises on membrane thinness or use of high crosslinker:elastomer base ratios, which render the membranes relatively difficult to stretch.

Silicone membranes are also typically 2–3 orders of magnitude stiffer than healthy lung tissue. Based on AFM nanoindentation studies,[15] the median Young's modulus of healthy murine lung parenchyma is 1.4 kPa, with rare locations exceeding 8.4 kPa. In contrast bleomycin-treated murine lung parenchyma, a model of pulmonary fibrosis, exhibits a higher, median Young's modulus of 8.4 kPa, with rare values exceeding 42 kPa. Rigid substrata increase intercellular tension,[13,18] and likely predispose cells to junction disruption upon biochemical or mechanical perturbation.

Here we describe a cell stretcher that enables dynamic imaging of pulmonary cell monolayers under conditions that more closely mimic the physiological environment. This stretcher device (i) generates homogenous, uniform equibiaxial strain, thereby mimicking deformations during respiration; (ii) uses membranes with physiological and pathological stiffness; and (iii) enables dynamic, fluorescence imaging of cells during mechanical and biochemical perturbations. The design is based on reported equibiaxial strain-generating devices that model *in vitro* cyclic strain in organs such as the lung.[10,26] We further designed hybrid membranes with improved optical properties over commercial silicone. To mimic tissue stiffness, polyacrylamide gels were grafted to the hybrid membranes.[23,25] Time-lapse images of thrombin-treated pulmonary endothelial monolayers on cyclically stretched substrata revealed the dynamics of monolayer disruption and recovery, coordinate protective roles of both physiological CS and substrate stiffness, and their influence on cytoskeletal remodeling.

MATERIALS AND METHODS

Cell Culture and Reagents

Human pulmonary artery endothelial cells (HPAECs) were from Lonza (Walkersville, MD), cultured in the recommended endothelial cell growth medium EGM-2 (Lonza) with 10% (v/v) fetal bovine serum (Sigma-Aldrich, St. Louis, MO) in a humidified incubator at 37 °C at 5% CO_2. The third generation self-inactivating lentiviral plasmid for mCherry-Life-Act in a pLV-CMV-IRES-Puro backbone[11] was a gift from Johan de Rooij (UMC Utrecht, The Netherlands). The envelope plasmid PMD2.G and the packaging plasmid psPAX2 were from Didier Trono (Addgene plasmids #12259 and 12260, respectively). Lentivirally transduced HPAECs expressing mCherry-LifeAct (see Supplementary Information) were used for all experiments at passages 8–9. Collagen-I (Col-I) from rat tail was obtained from BD Biosciences (San Jose, CA) and human fibronectin (Fn) was from EMD Millipore (Temecula, CA).

Equibiaxial Stretcher Design

The stretcher is based on a previously reported design.[10] An elastic membrane (see below) is mounted onto a circular membrane-holding ring (MHR, inner diameter 44 mm, anodized aluminum, Fig. 1a) using a silicone O-ring (1.864" actual ID, 0.07" actual width, McMaster Carr, Elmhurst, IL) that fits into a groove (1.78 mm width) in the base of the MHR. The MHR stretches the membrane over a fixed indenter ring (IR, outer diameter 41 mm, anodized aluminum, Fig. 1b) and exerts equibiaxial strain on the flat section of the membrane. The use of an indenting ring, as opposed to a post, enables membrane imaging with an inverted fluorescence microscope. Because the IR is immobile during strain, there is negligible membrane z-movement, and the membrane remains in the same focal plane (Figs. 1c and 2e). The MHR is mounted on an aluminum arm with a linear actuator (Anaheim Automation, 11AV102AX06, Anaheim, CA) at one end to move the MHR vertically over the IR (Fig. 1c). The other end moves along a Frelon-lined guide rail, ensuring smooth, vertical movement. The edge of the mounted membrane is lubricated with food-grade silicone grease (Refrigeration Technologies, Fullerton, CA) to reduce friction between the membrane and IR, during indentation (Fig. 2e). The center of the membrane supporting cells is free of lubricant and optically transparent. The stretcher base is designed to mount on the stage of a Zeiss Axiovert 200 M epifluorescence microscope for dynamic imaging of cells subjected to equibiaxial strain (Figs. 1c and 2e). A programmable driver controls the linear actuator (EZStepper EZ17, Allmotion, Union City, CA). Cyclic strain (CS) is applied in a triangular wave with desired amplitude and frequency, and can be paused at any time or indentation depth for imaging.

Hybrid Membrane Fabrication

Hybrid membranes were fabricated using medical-grade silicone sheeting (0.01'' nominal thickness, SMI silicone, Saginaw, MI) as a scaffold to ensure mechanical durability at the edges where the membranes are mounted onto the MHR. The scaffold experiences significant tensile, compressive and shear forces, during mounting and indentation. A mask was formed by excising a 40 mm diameter circle from the center of a 60 mm × 60 mm silicone sheet. After placing the mask on a glass slab, a thin, transparent PDMS film was cast in the central cut out region, as an optical window, by pouring ~0.63 g of 26:1 (w/w) elastomer base:crosslinker PDMS (Sylgard 184, Dow Corning, Auburn, MI) into the cut out region, with a 1 mm edge overlap with the silicone sheeting (Fig. 2a). This assembly was cured for 14–16 h at 65 °C, and the hybrid membrane was peeled off the glass and placed on an inverted MHR. Holding the membrane under slight tension, the silicone scaffold was fit into the groove of the MHR with the O-ring. Excess silicone was removed (Fig. 2b).

The membrane-mounted MHR can be autoclaved and directly used for cell culture. On a 1 cm diameter spot in the center of the membrane, 150 μL of 50 μg/mL Fn or Col-I was incubated for 1 h at 37 °C. Then, ~25,000 HPAECs expressing mCherry-LifeAct were seeded on the same spot with 150 μL of medium. After 2 h, once the cells attached and started spreading, 4 mL medium was added to the MHR.

Grafted Polyacrylamide Hydrogels on PDMS Membranes

To mimic tissue stiffness, polyacrylamide hydrogels were grafted onto hybrid membranes, using benzophenone photochemistry.[23,28] A 10% (w/v) solution of benzophenone in 30:70 (v/v) water:acetone was incubated on the PDMS window of a hybrid membrane for 1 min, rinsed with methanol, and air-dried. Then, 15 μL of a solution containing acrylamide and bis-acrylamide at desired concentrations, 0.05% ammonium persulfate, and 0.5% TEMED (Bio-Rad, Hercules, CA) in PBS was pipetted onto the center of the treated membrane, and a 12 mm glass coverslip was placed over it. The assembly was exposed to UV light (360 nm, 4.4 mW/cm^2, Spectroline XX-15A benchtop UV lamp) for 45 min, to cure the gels and graft them to the PDMS (Fig. 2d). To prevent oxygen from diffusing through the thin PDMS membranes (< 200 μm) and inhibiting polymerization, a 25 mm glass coverslip was placed on the underside of the membrane. We grafted hydrogels with nominal Young's moduli of 5 kPa (5% acrylamide and 0.15%

bis-acrylamide, (w/v)) and 15 kPa (10% acrylamide and 0.3% bis-acrylamide, (w/v)) (see Supplementary Information), which are within the respective stiffness ranges for normal and fibrotic lung tissue.[15]

After polymerization, the membrane was immersed in PBS, and the coverslips were gently released after 10 min of hydrogel swelling. The hydrogels were twice treated with 0.05% (w/v) Sulfo-SANPAH (ProteoChem, Loves Park, IL) in PBS under 360 nm UV (1.85 J/cm^2 per exposure), with PBS rinses between treatments.[21] Col-I (200 μg/mL in PBS) was covalently linked to the activated hydrogels by incubation for 3 h at 37 °C. Treated hydrogels were stored overnight at 4 °C under PBS containing 1% penicillin–streptomycin. The next day, gels were rinsed with warmed medium, and mCherry-LifeAct expressing HPAECs were seeded on hydrogels, as with PDMS membranes (Fig. 2e).

Preconditioning HPAECs to Cyclic Strain

Cells seeded on membranes were cultured to confluence in the incubator over 2 days. To precondition EC monolayers outside the incubator, a heated enclosure maintained the temperature at 37 $\pm$ 1 °C. Cells were cultured in EGM-2 medium, buffered with 25 mM HEPES, 2 mM sodium pyruvate to neutralize HEPES phototoxicity[24] and 1% penicillin–streptomycin. Humidity was maintained by bubbling air through DI water. Under these conditions, cells in tissue culture dishes survived and proliferated for at least 48 h (not tested further). However, for the cyclic strain experiments, the exposed underside of the thin membrane increases evaporation. Thus during preconditioning, a plastic plug was used with the IR to reduce membrane exposure to air (Fig. 1b). Sterile DI water was also periodically added to medium covering monolayers, to maintain osmolarity against evaporation.

The MHR was covered with a 60 mm tissue culture dish cover, sealed with Parafilm (Bemis Company, Neenah, WI), and mounted onto the aluminum arm of the stretcher at the relaxed position (Figs. 1c and 2e). This static preconditioning lasted 12–16 h. Subsequently, the medium was replaced, and cells were preconditioned with 8 h of either 5% linear equibiaxial CS at 15 cycles/min or no CS (static) (Fig. 4a). A 5% linear strain approximates physiological levels of strain in lungs,[2,26] and 15 cycles/min is within the range of adult human respiration rates.

Live-Cell Imaging of Cyclically Stretched Monolayers

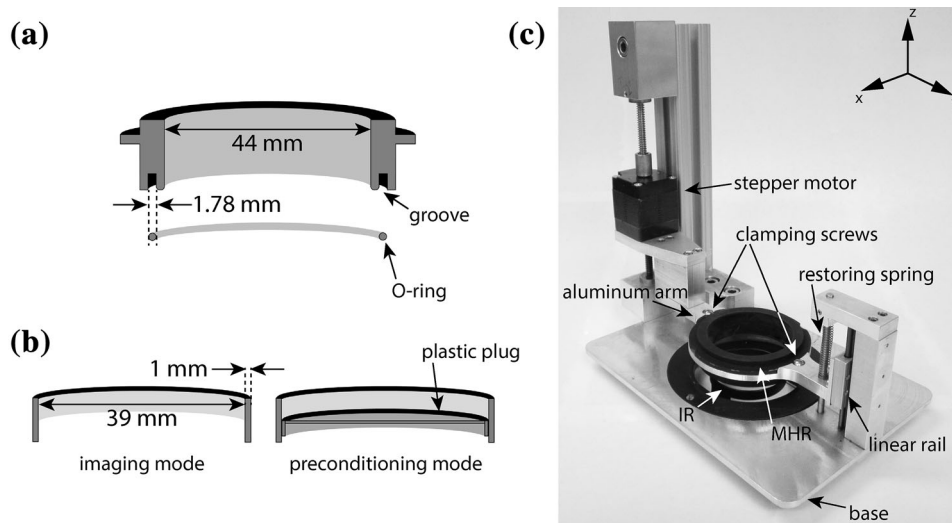The plastic plug was removed from the IR, and the stretcher was mounted on a Zeiss Axiovert 200 M

FIGURE 1. Design of equibiaxial cell stretcher. (a) Cutaway view and dimensions of an anodized-aluminum Membrane-Holding Ring (MHR). An O-ring fits into a groove in the base of the MHR and is used to mount membranes on the MHR. The metal lip on the outside of the MHR is used to clamp the MHR to the aluminum arm of the stretcher with two diametrically opposite screws. (b) Cutaway view and dimensions of the anodized aluminum Indenting Ring (IR). The use of a ring facilitates imaging, as opposed to a cylindrical post, but this configuration increases evaporation losses due to the exposed membrane. Evaporation losses can be reduced using a plastic plug during stretch-preconditioning, in order to reduce membrane exposure to atmosphere. (c) Image of the cell stretcher showing an MHR clamped onto the aluminum arm, and positioned over the IR. On opposite sides of the aluminum arm are the stepper motor driving the arm, and a linear rail which guides the arm. The base of the device is designed to be mounted on a microscope stage.

inverted epifluorescence microscope with a motorized stage and a 20 × air objective (NA = 0.50). The microscope was in a heated enclosure. The preconditioned MHR was mounted on the stretcher, CS was applied for 20 min, and 3–4 monolayer locations 1–5 mm apart were chosen for tracking (Fig. 4a). Phase contrast and fluorescence images were taken at defined intervals. At 25 min after initiating image acquisition, human α-thrombin (Enzyme Research Laboratories, South Bend, IN) was added at $t = 0$ min to a final concentration of 0.1 U/mL, and images were acquired for $t = 145$ min, while continuing CS between acquisition time points. Images were acquired 2 min after pausing CS, to allow system stabilization.

Optical Comparison of Commercial Silicone and PDMS

To quantify background fluorescence from different membranes, five sections each of commercial silicone sheeting and central PDMS window were imaged under identical conditions, with fluorescence filter sets for FITC and Rhodamine channels. Images acquired without illumination accounted for the dark current.

Membrane sections, two of each type, were also incubated with 20 μg/mL fibronectin, seeded sparsely with HPAECs and incubated for 1 day. Cells were fixed with 4% paraformaldehyde (Fisher), permeabilized with 0.1% (v/v) Triton X-100 (Sigma), blocked with 1% (w/v) BSA, stained with Alexa Fluor 488-phalloidin (Molecular Probes) and mounted on a glass slide. F-actin was imaged through the membranes, under identical conditions.

Image Analysis and Statistical Testing

For studies of gap dynamics, monolayer images were analyzed with ImageJ v1.50a (NIH). At each location, we compiled a stack of phase contrast images from all time points, to generate a time-lapse movie of the thrombin-treated EC monolayer. Two separate 150 μm × 150 μm fields were randomly chosen per stack, and gaps in the monolayer were outlined and quantified. We thus report average gap areas per 22,500 μm² field. Per field, the gap formation rate was also calculated between two consecutive time points t_i and t_{i+1}, and averaged,

$$\text{Gap formation rate} = \frac{\text{Gap}(t_{i+1}) - \text{Gap}(t_i)}{t_{i+1} - t_i}$$

For monolayers on hydrogels of different moduli, $n = 18$ fields from three independent experiments were imaged per condition per time point. Because studies involved variations in both stiffness and mechanical strain, at each time point we performed an ANOVA to detect significant effects ($\alpha = 0.05$). The gap areas and formation rates were distributed non-normally, but
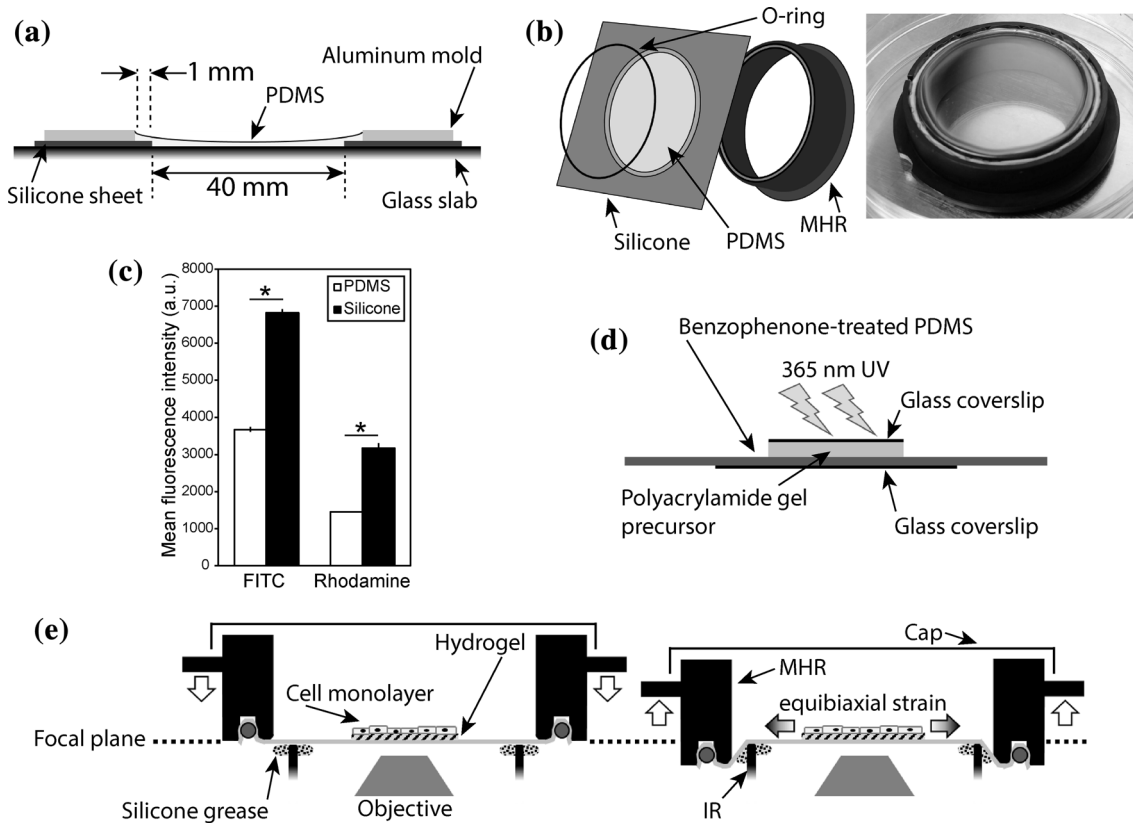
FIGURE 2. Fabrication and performance of hybrid membrane, gel-grafting, and equibiaxial strain schematic. (a) Hybrid membranes were fabricated by casting polydimethylsiloxane (PDMS) of 26:1 (w/w) elastomer base:crosslinker ratio into the central cutout area of a silicone sheet, against a flat glass slab, confined by an aluminum mold. (b) Hybrid membranes with durable silicone backbones and optically clear, compliant central windows were mounted onto MHRs by O-rings. (c) Under the same imaging conditions, the average background mean fluorescence intensity of the hybrid membrane (PDMS window) and the silicone sheet were quantified using two different filter sets. The hybrid membrane showed half the background intensity of the commercial silicone sheet. Error bars are SEM. Asterisks (*) represents $p < 5 \times 10^{-12}$, n = 25 regions of interest from 5 independent membranes. See also Fig. S1. (d) During polyacrylamide gel grafting, a glass coverslip backing was necessary to prevent oxygen-inhibition of gel polymerization. (e) During cyclic indentation of the MHR by the IR, the cell monolayer cultured on the hydrogel senses the gel stiffness and the equibiaxial strain. Silicone grease at edge of the membrane reduces friction between the membrane and the IR.

unimodally. Because variance homogeneity could not be established for the four different conditions, Brown-Forsythe's modification to the two-way ANOVA was preferred.[6] For monolayers on hybrid membranes, we compared n = 14 fields each, from two independent experiments per condition per time point, using a one-tailed Welch's t test with unequal variances ($\alpha = 0.05$) to identify significant effects of 5% CS. The same test was used in all other comparisons.

To quantify fluorescence background from membranes, in each channel, an image stack was compiled consisting of (i) the dark current image, (ii) five PDMS section images, and (iii) five commercial silicone section images. Per stack, five well-spaced 150 pixel × 150 pixel regions of interest (ROI) were defined, and mean fluorescence intensities (MFI) were measured. For each channel,

$$\text{Background MFI}_{i,j,k} = \text{MFI}_{i,j,k} - \text{Dark Current MFI}_k$$

Here, i = membrane type; j = 1, 2... 5, independent membrane sections; k = 1, 2... 5, ROIs. For each channel, averaging across n = 25 ROIs from five independent sections,

$$\text{Average Background MFI}_i = \frac{\sum_j \sum_k \text{Background MFI}_{i,j,k}}{5 * 5}$$

All data are reported as the mean ± SEM.

Strain Characterization

Fluospheres (0.2 μm diameter, 580 nm/605 nm red fluorescent beads; Molecular Probes, ThermoFisher Scientific; Eugene, OR) were added 1:1000 (v/v) to the hydrogel precursor solution. The MHR was inverted during gel grafting to promote bead accumulation at the free surface of the hydrogel. Hybrid membranes

with grafted hydrogels were indented incrementally, from the relaxed position. At each step, fluorescent beads at the top surface of the gels and microscopic features in the PDMS membrane directly underneath were imaged, by fluorescence and phase contrast, respectively. At the gel top and PDMS bottom, linear strains were calculated along orthogonal axes. The ratio of strains at the gel top and PDMS bottom determined the strain transfer ratio. Averaging across five independent membranes, the linear strains at the gel surface, and the strain transfer ratios were plotted against indentation depth.

To verify equibiaxial strain, for each of the eight membranes subjected to CS, microscopic features in the PDMS membrane were phase contrast imaged at the relaxed and 5% linear strain positions. A central 'origin' was defined in the relaxed image, four axes offset by 45° were drawn, and two points were chosen per axis on either side of the origin (Figs. 3c and 3d). Measuring the distances from the origin to each point, before and after indentation, the linear strain along each axis was calculated and averaged across the eight membranes.

RESULTS

Hybrid Membranes Exhibit Improved Image Quality and Durability

Autofluorescence from the commercial silicone membrane was nearly twice that of the thin PDMS window in our hybrid membranes (Fig. 2c). The reduced background from our hybrid membranes was also noticeable in fluorescent images of stained F-actin (Fig. S1), and would benefit quantitative comparisons of fluorescence images of cells. The hybrid membranes also sustained continuous 10% linear equibiaxial CS at 15 cycles/min for 24 h (not tested further) without any evidence of mechanical failure.

Homogeneity of Equibiaxial Substrate Strain

The hydrogel grafting was very robust. After 24 h of 10% linear, equibiaxial CS at 15 cycles/min, only negligible cracks at the gel-PDMS interface were seen at the gel perimeter, with no bulk damage. The calibration revealed a maximum possible $11 \pm 2\%$ linear strain with the current configuration (Fig. 3a), but a redesigned MHR or IR could increase the strain limit. The thicknesses of the soft and stiff grafted hydrogels, determined by phase contrast microscopy, were 78 ± 4 and 81 ± 6 μm respectively ($n = 6$ gels each, $p = 0.72$). We further verified that the strain transfer ratio between the PDMS and gels was ~1 (Fig. 3b), in

agreement with previous reports.[23] At 5% CS, the spatial distribution of the strain profile was essentially homogenous, with a minimum strain of $5.3 \pm 0.3\%$ along the 135°–315° direction and a maximum strain of $5.9 \pm 0.5\%$ along the 45°–225° direction ($p = 0.13$) (Fig. 3e).

Dynamic Imaging Reveals the Protective Effects of Cyclic Stretch on Endothelial Monolayers

When EC monolayers on fibronectin-coated hybrid membranes were subjected to eight hours of 5% CS prior to thrombin stimulation, the mechanical stimulation alone induced some gap formation (Fig. S2A). Five minutes prior to thrombin treatment, static samples exhibited gap areas of 10 ± 5 μm^2/field, whereas 5% CS samples exhibited substantially larger gaps, 120 ± 30 μm^2/field (Table S1, $p = 2.7 \times 10^{-3}$). Presumably these gaps heal under persistent CS (> 8 h), as cell division replaces dead cells.[2,16]

On hybrid membranes, 5 min after thrombin stimulation, the average gap areas in static and stretched samples were nearly identical (Fig. S2A). However at 15 min when gap areas peaked, the gaps in static monolayers (6800 ± 600 μm^2/field) were 144% larger than in 5% CS treated monolayers (2800 ± 400 μm^2/field, $p = 5.0 \times 10^{-6}$). Lamellipodia were already visible at 15 min, and monolayer recovery was apparent at 25 min (Supp. Videos 1, 2, Fig. S2A). The gap areas in static and stretched monolayers respectively decreased to 2800 ± 400 μm^2/field and 600 ± 100 μm^2/field ($p = 1.8 \times 10^{-5}$), i.e., 41 and 23% of the respective peak values. At 55 min, gap areas in the static monolayers were 150 ± 80 μm^2/field, which appears greater than the stretched monolayers (40 ± 20 μm^2/field), although statistical significance could not be established ($p = 0.08$). Within 115 min, gap areas in all conditions returned to pre-thrombin levels.

An advantage of our device is the ability to track specific fields over time, enabling reliable calculation of the gap formation rate. In the -5 to 5 min interval, the average gap formation rates (Fig. S2B, Table S2) for static and stretched samples were comparable, 170 ± 30 μm^2/min-field and 160 ± 30 μm^2/min-field respectively ($p = 0.37$). However, the rate during 5–15 min increased to 510 ± 60 μm^2/min-field in static samples, whereas it decreased in stretched samples to 110 ± 30 μm^2/min-field ($p = 1.03 \times 10^{-5}$), indicating the initiation of monolayer recovery mechanisms in the stretched samples. Over subsequent intervals, the average rate remained significantly more negative for the static samples. We attribute the latter to the larger peak gap area in static samples.
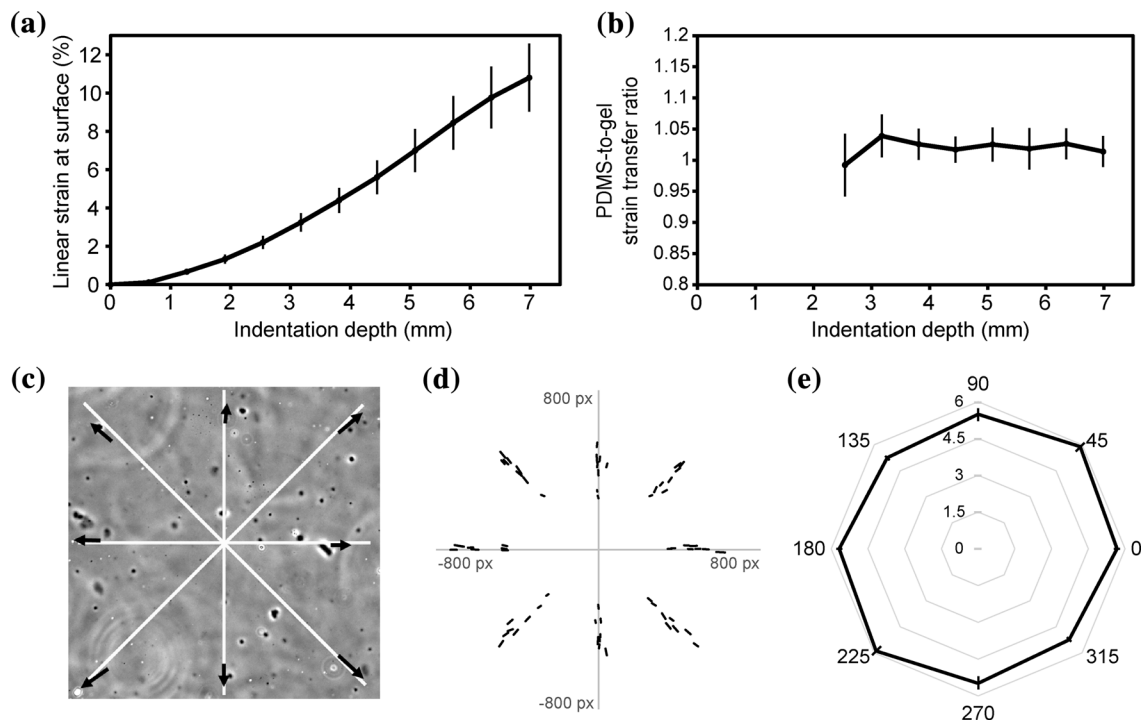
FIGURE 3. Membrane strain characterization. (a) Fluorescent microspheres near the surface of the hydrogel were imaged at different indentation depths (membrane stretch) to calculate the linear strain averaged along two orthogonal axes. (b) Microscopic features on the PDMS membrane were also imaged and strains calculated. The calculated strain transfer ratio ($\varepsilon_{gel}/\varepsilon_{PDMS}$) was ~1 (at low strains, data were too noisy due to small denominators and are not shown). Data in panels A and B are the pooled average of $n = 3$ membranes with 5 kPa gels and 2 with 15 kPa gels. (c, d) Microscopic features on the PDMS were tracked along the four indicated axes, in order to determine the strain homogeneity, at the ~5% strain condition. Results from n = 8 membranes are shown in panels d and e. The linear strain varies between 5.9% (45°–225°) and 5.3% (135°–315°), but the difference is not statistically significant. All error bars are SEM.

It is worth noting that on Col-I coated hybrid membranes, confluent EC monolayers formed as expected and tolerated 5% CS. However, upon thrombin stimulation, the monolayers peeled off the substrate under both static and 5% CS conditions. We attribute this behavior to delamination of physisorbed collagen by contractile cells because, on hydrogels with covalently bound Col-I, thrombin treated monolayers remained attached to the substrate.

These data demonstrated the protective effect of cyclic stretch on EC monolayers, previously established with fixed monolayers on uniaxially stretched silicone substrates.[3] The results not only validated our stretcher and hybrid membrane for dynamically imaging cyclically stretched monolayers, but also revealed additional details of gap formation and reannealing.

Substrate Rigidity Alters Thrombin Induced Gap Formation in Static and Cyclically Stretched Monolayers

To first assess the impact of substrate rigidity on thrombin-induced gap formation, we compared static

EC monolayers on 5 and 15 kPa gels. Figure 4b plots the interendothelial gap area following thrombin stimulation at $t = 0$ min. At -5 and 5 min, gap areas in static EC monolayers on 5 and 15 kPa gels were similar, with evident gaps at 5 min (Table 1, Supp. Video 3). However, at 15, 25, and 55 min, the gap areas were significantly smaller in monolayers on the softer hydrogels, in qualitative agreement with literature.[13] Substrate stiffness also affected the gap formation rates in static monolayers (Fig. 4c; Table 2). Between 5 and 15 min, the gap formation rate was higher for the stiff substrate. During recovery, between 25 and 55 min and 55 and 115 min, gap formation rates were more negative in monolayers recovering from larger gaps, i.e., on stiff substrates.

To investigate the combined influence of cyclic stretch and substrate stiffness on thrombin-induced gap formation and recovery dynamics, EC monolayers on grafted hydrogels were subject to 5% CS, as above. Prior to thrombin stimulation, the gap areas in 5% CS-treated monolayers, were again significantly larger than in static monolayers, regardless of the matrix stiffness (Fig. 4b; Table 1). However in all cases, there were prominent stress fibers and F-actin at the cell
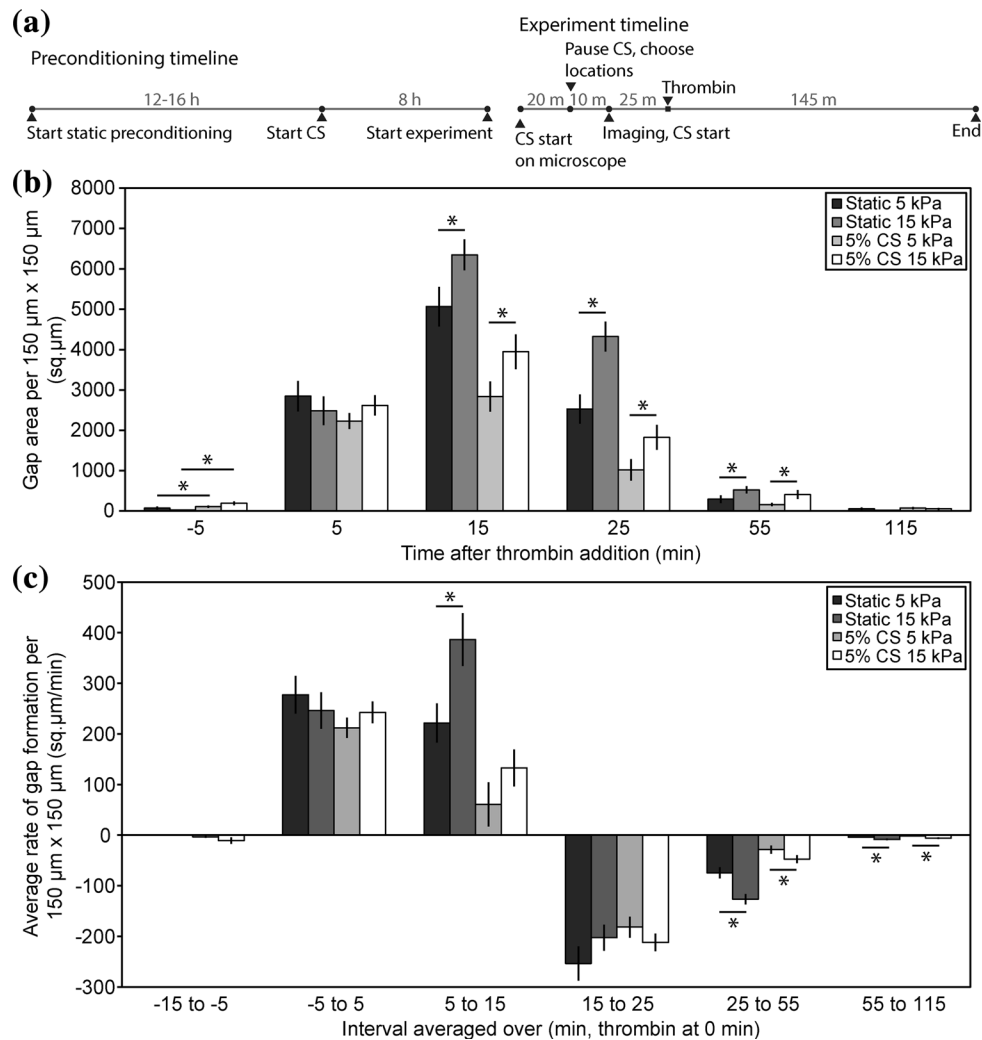
FIGURE 4. Gap dynamics on collagen-coated soft and stiff hydrogels after thrombin stimulation. (a) Cell monolayers were preconditioned for culturing outside the incubator for 12–16 h, before being subjected to 8 h of equibiaxial 5% CS. After mounting the stretcher with the cell monolayer on the microscope, cells were subjected to CS for 20 min before locating 3–4 positions to track over time. Images were taken every 10–30 min during programmed breaks in cyclic strain application. (b) Average gap area per 150 μm × 150 μm field is plotted as a function of time after thrombin addition to endothelial monolayers cultured on 5 and 15 kPa Collagen-I coated hydrogels. Gaps are greatest at 15 min. (c) Average gap formation rate in the same fields is presented for different intervals. From the second to the third interval, all gap formation rates fall except for the static, 15 kPa substrate. Asterisks (*) indicates only specific significant comparisons described in the text, within individual time points or intervals. Statistical information on effects of matrix stiffness and CS are summarized in Tables 1 and 2 respectively. Per condition, $n = 18$ fields from 3 independent experiments. Error bars are SEM.

TABLE 1. p values for Main effect and Interaction effect at different time points from Brown-Forsythe's modified ANOVA analysis of EC monolayer gap areas on Collagen-I coated hydrogels.

Time point (min)	Calculated df_{Error}	Main effect cyclic strain (C)	Main effect matrix stiffness (M)	Interaction effect (CM)
−5 min	27.10	0.021	0.39	0.08
5 min	55.89	0.43	0.96	0.22
15 min	64.79	7.6E−07	6.1E−03	0.84
25 min	63.85	7.7E−08	2.0E−04	0.14
55 min	55.44	0.17	9.9E−03	0.93
115 min	52.50	0.33	0.34	0.77

Thrombin was added at $t = 0$ min.

TABLE 2. *p* values for Main effect and Interaction effect from Brown-Forsythe's modified ANOVA analysis of gap formation rates over different intervals in EC monolayers on Collagen-I coated hydrogels.

Interval (min)	Calculated df_{Error}	Main effect cyclic strain (C)	Main effect matrix stiffness (M)	Interaction effect (CM)
−15 to −5 min	21.75	0.035	0.25	0.32
−5 to 5 min	53.70	0.25	0.99	0.30
5 to 15 min	62.71	1.03E−05	8.0E−03	0.29
15 to 25 min	54.41	0.22	0.68	0.11
25 to 55 min	62.87	7.6E−09	3.5E−04	0.079
55 to 115 min	61.46	0.068	1.7E−03	0.99

Thrombin was added at $t = 0$ min.

periphery (Fig. 5, Supp. Videos 3, 4). Five minutes after thrombin challenge, interendothelial gaps under all four conditions were comparable. The increase in gap areas also coincided with the dissolution of stress fibers, retraction of the cell periphery, and cell–cell junction remodeling.

At 15 min, gap areas peaked across all four conditions (Fig. 4b). The gap areas in stretched monolayers on 15 kPa substrates were 3900 ± 400 μm^2/field compared to 2800 ± 400 μm^2/field on 5 kPa—a statistically significant increase of 39% (Table 1). Active lamellipodia were visible at 15 min and with cell–cell contacts being re-established, the gaps decreased at 25 min (Fig. 5, Supp. Videos 3, 4). The protective effects of both softer matrix and CS remained statistically significant during this early recovery stage. In stretched monolayers, the gap areas on 15 kPa substrates (1800 ± 300 μm^2/field) were 79% greater than on 5 kPa substrates (1000 ± 300 μm^2/field). At 55 min (late recovery stage), only the substrate stiffness appeared to have a significant effect on monolayer recovery (Table 1). The gap areas on stretched 15 kPa gels (400 ± 100 μm^2/field) were 153% larger than on stretched 5 kPa gels (160 ± 40 μm^2/field). At 115 min, the gaps in EC monolayers under all conditions were minimal and comparable.

In the intervals −5 to 5 min and 15–25 min, gap formation rates were comparable across all four conditions (Fig. 4c; Table 2). However between 5 and 15 min in stretched monolayers, while gap formation rate on 5 kPa gels (60 ± 40 μm^2/min-field) was 55% lower than on 15 kPa gels (130 ± 40 μm^2/min-field), and the effect of substrate stiffness was significant, the error bars do overlap slightly. Between 25–55 min and 55–115 min, substrate stiffness significantly affected the gap formation rate. In fact between 55 and 115 min, stiffness was the single mechanical parameter affecting the gap formation rate (Table 2).

It is worth noting that the peak monolayer gap areas were smallest on stretched 5 kPa gels, and largest on static 15 kPa gels (Fig. 4b). The latter were also the only monolayers which showed an increase in the gap formation rate between 5 and 15 min (Fig. 4c,

390 ± 50 μm^2/min-field), over the previous time interval (−5 to 5 min, 250 ± 40 μm^2/min-field)—all other conditions showed a reduction in gap formation rates during this interval. This was accompanied by reduced lamellipodial activity at 15 min in monolayers on static 15 kPa gels, relative to other conditions (Fig. 5, Supp. Videos 3, 4).

We also observed apparent solvent blisters underneath the EC monolayer (Fig. 6, Supp. Video 5), immediately after 3 min of 5% CS on grafted hydrogels. Blisters were typically observed beneath the cell body, and dissipated within ~50 s. They were not observed underneath monolayers on PDMS. Similar behavior was reported in epithelial cell monolayers on hydrogels, upon sudden relaxation after single stretch of 5% or greater equibiaxial strain for longer than 1 min.[7] Such behavior was attributed to increased solvent pressure at the basal plane due to liquid efflux from porous hydrogels on relaxation, with greater basal solvent pressure on stiffer hydrogels, and thus larger blisters. Thus, CS-treated EC monolayers on hydrogels may also experience additional cyclic hydrodynamic pressure across the monolayer.

DISCUSSION

We report the development of a live-cell-imaging-capable equibiaxial cell stretcher and hybrid membranes with improved optical properties for use with this device. Results obtained with this platform demonstrated that physiological substrate stiffness and cyclic strain coordinately protect the endothelial monolayer against thrombin-induced disruption.

The described hybrid membranes exhibited uniform equibiaxial strain (Fig. 3e), and remained within the focal plane during stretching, enabling live cell imaging during sustained cyclic stretch. These membranes combine the advantages of PDMS and silicone. The PDMS optical window autofluorescence was 50% lower than commercial silicone (Fig. 2c). The outer, commercial silicone scaffold provided the necessary durability to withstand stretching while mounted on
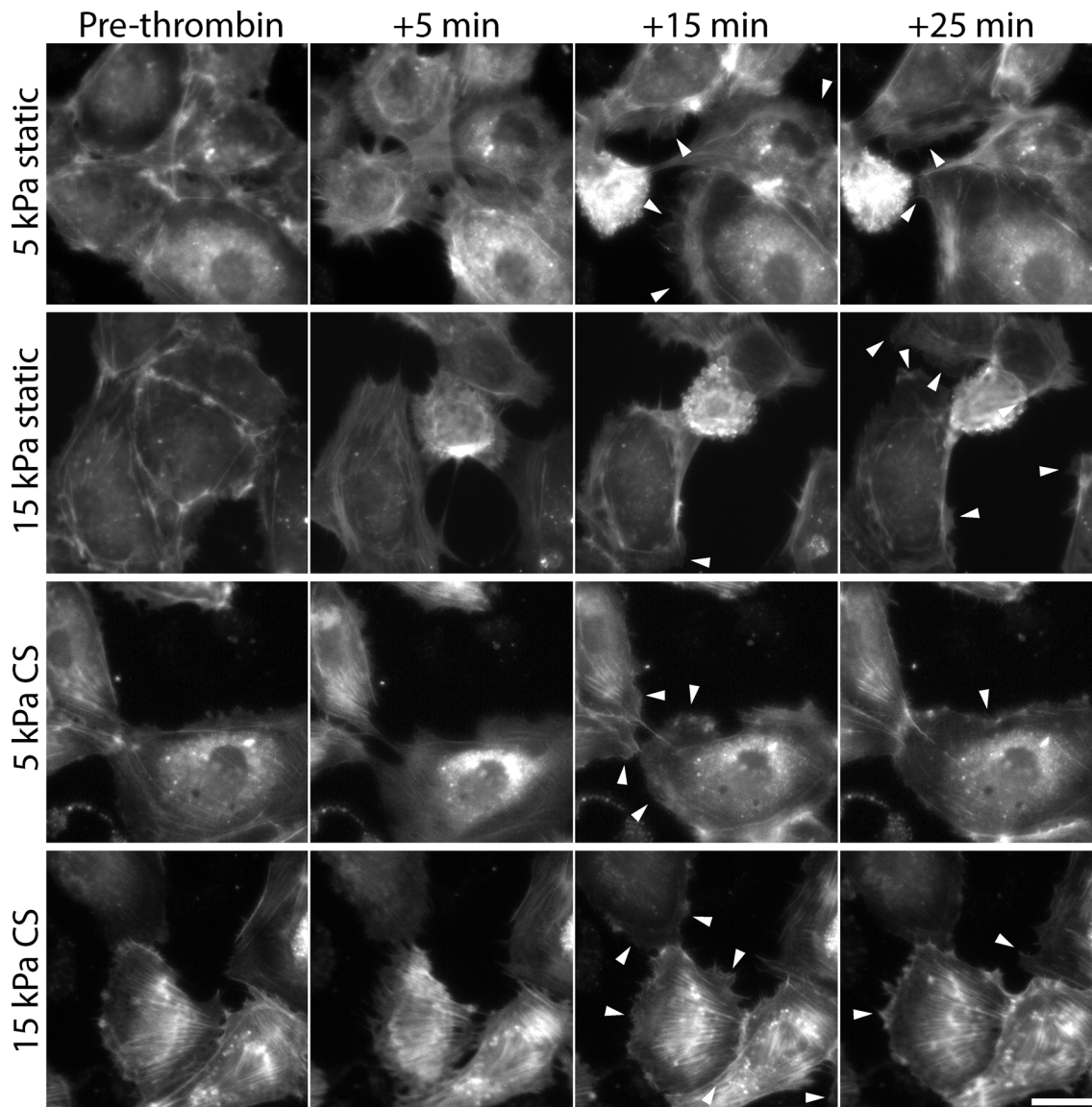
FIGURE 5. Live cell imaging of actin dynamics as a function of time, relative to thrombin treatment. Representative images of mCherry-LifeAct visualized in HPAEC monolayers shows dissolution of stress fibers at 5 min post-thrombin stimulation, and corresponding retraction of the cell edge. Lamellipodia (white arrows) are apparent at 15 min under most conditions, but this is delayed to 25 min in the static monolayers on 15 kPa gels. Representative images from $n = 18$ fields from 3 independent experiments per condition. Scale bar 25 μm. See also Supp. Videos 3 and 4.

the MHR. Hydrogels grafted to the PDMS window enabled greater control over the substrate stiffness, while ensuring 100% strain transfer between the PDMS and hydrogel (Fig. 3b).

Treatment with the serine protease thrombin increases cell actomyosin contractility by Rho/Rho kinase-mediated inhibition of myosin light chain phosphatase activity.[2,8] This contractility and associated signaling induces endothelial monolayer gap formation, which is mitigated by factors that reduce RhoA activity.[2,13] Conversely, Rac-mediated cortactin accumulation, actin polymerization, and lamellipodia formation at the cell periphery enable monolayer recovery, which is

enhanced by Rac activation.[3] The influence of cyclic strain and substrate stiffness on thrombin actuated endothelial disruption and resealing have been studied independently, in the context of endothelial monolayer integrity and barrier function.[2–5,12,13]

Uniaxial cyclic strain influences cell orientation and proliferation in pulmonary endothelial monolayers.[2,16] Relative to static monolayers, 5% uniaxial CS reduced interendothelial gaps observed 50 min after thrombin treatment, but not at 5 min, suggesting faster monolayer recovery in stretched monolayers.[3] The latter behavior was accompanied by increased focal adhesion staining and cortactin accumulation near the cell
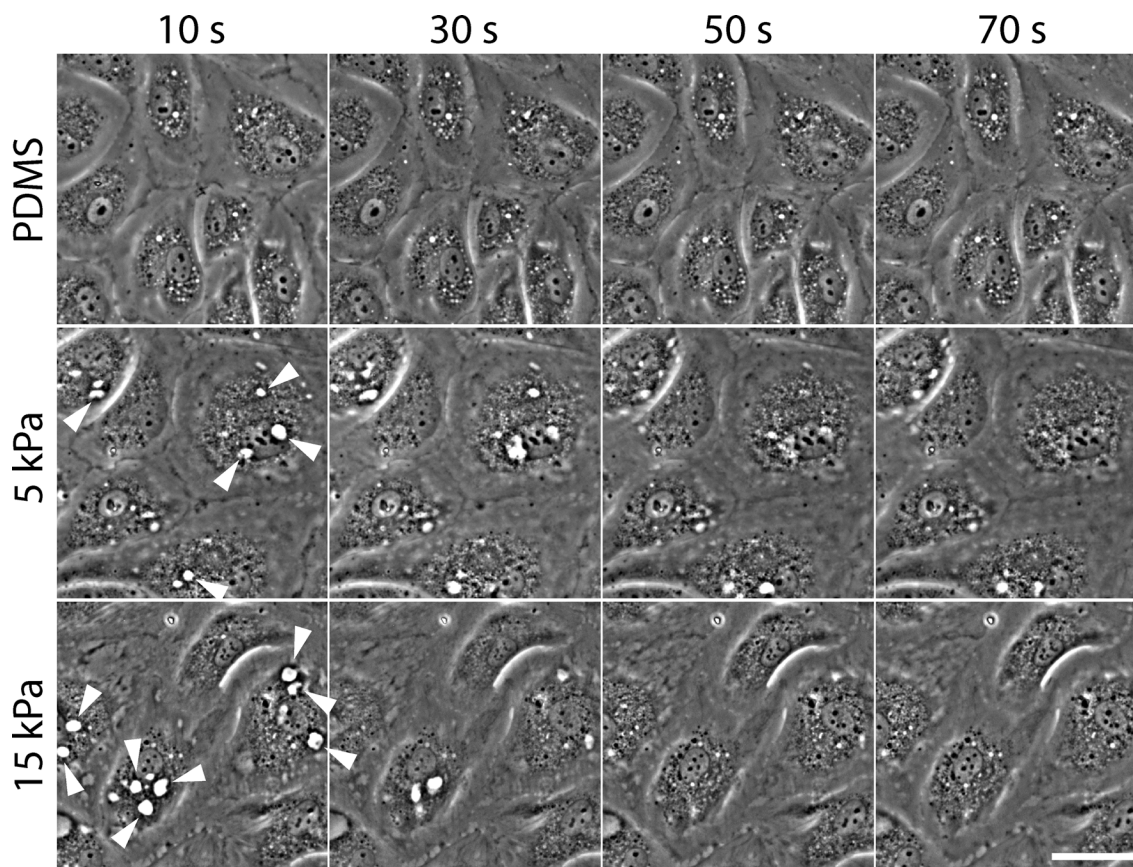
FIGURE 6. Formation of solvent 'blisters' beneath cells, attributed to porous flow out of hydrogels. HPAEC monolayers were subjected to 3 min of 5% CS at 15 cycles/min, and then immediately imaged by phase contrast microscopy every 10 s for 80 s. In cell monolayers cultured on hydrogels, bright spots beneath cells (white arrows) formed and dissipated over 50 s. These spots do not appear under monolayers cultured on PDMS, which lacks water-permeable pores. Representative images from $n = 4$ fields from 2 independent experiments per condition. Scale bar 40 μm. See also Supp. Video 5.

periphery.[3] Chronic preconditioning with uniaxial 5% CS also reduced RhoA activation 5 min post-thrombin stimulation, and increased Rac1 activity at 50 min, relative to static controls.[3] Our live-cell imaging results obtained with hybrid membranes and grafted hydrogels indicate similar gap formation trends for stretched vs. static monolayers, including the protective effect of CS and the presence of lamellipodia during recovery (Figs. S2A, 4b and 5). Our measurements revealed additional differences in monolayer disruption and recovery dynamics at multiple time points. Specifically, the largest gaps were evident 15 min after thrombin, with recovery apparent within 25 min for all conditions. The imaging capability of our device enabled the dynamic tracking of multiple specific fields per membrane, and thus significantly reduced experimental variability, while enabling visualization of subcellular processes and comparisons of the gap formation rates under different conditions over 3 h observation time (Fig. S2B). Eliminating the need for fixation also increased throughput and avoided potential artifacts associated with fixation and staining.

Studies of static monolayers demonstrated higher Rho-kinase dependent cell contractility on stiff substrata, with corresponding increases in stress fiber formation,[5] monolayer forces[13] and leakier junctions.[12] Thus in prior studies, cells cultured on stiff elastomeric membranes likely had elevated levels of active RhoA, relative to cells in pulmonary tissue. Thrombin treatment also increased Rho kinase-dependent stress fiber and gap formation on stiff matrices relative to soft ones.[5,13] Our results with static monolayers similarly demonstrated increased gap formation on 15 kPa hydrogels relative to 5 kPa, but we also showed that the effect was mitigated by equibiaxial 5% CS (Fig. 4b). Importantly, physiologically relevant substrate stiffness and cyclic stretch together had a greater protective effect against agonist challenge. We further showed that the attenuation in the gap formation rate, indicative of monolayer recovery, was delayed to the 15–25 min interval in monolayers on static 15 kPa substrates, relative to other conditions (Fig. 4c). Fifteen minutes after thrombin addition, even as gap areas increased, prominent lamellipodia were visible

for all conditions, except on the static 15 kPa substrates (Fig. 5, Supp. Videos 3, 4). Further, at the 55 min time point (Fig. 4b), only the softer substrate maintained a significant effect (Table 1), suggesting that stretched monolayers on 5 kPa gels completed resealing earlier than on 15 kPa gels (Fig. 4b). Our results thus establish that both physiological matrix stiffness and physiological cyclic stretch coordinate to protect pulmonary endothelial monolayers against disruption by inflammatory mediators such as thrombin.

These findings suggest that fibrotic lung tissue could augment pulmonary vascular leak triggered by inflammatory mediators and barrier agonists, and delay endothelial barrier recovery relative to healthy tissue. Hypoxia is believed to increase pulmonary tissue stiffness,[19] which is associated with disorders such as pulmonary fibrosis.[15] Genetic polymorphisms[1] and aging[12,27] can also contribute to vascular stiffening. The balance between cell–cell and cell-substrate adhesion and cell contractility is complex.[8] However, the device described here provides a platform for investigating their influence on endothelial function, and for interrogating the dynamic, subcellular mechanisms contributing to the mechanical regulation of the vascular endothelium.

ELECTRONIC SUPPLEMENTARY MATERIAL

ACKNOWLEDGMENTS

CONFLICT OF INTEREST

The authors report no conflicts of interest.

REFERENCES

[1]Agrotis, A. The genetic basis for altered blood vessel function in disease: large artery stiffening. *Vasc. Health Risk Manag.* 1:333–344, 2005.
[2]Birukov, K. G., J. R. Jacobson, A. A. Flores, S. Q. Ye, A. A. Birukova, A. D. Verin, and J. G. N. Garcia. Magnitude-dependent regulation of pulmonary endothelial cell barrier function by cyclic stretch. *Am. J. Physiol. Lung Cell. Mol. Physiol.* 285:L785–L797, 2003.
[3]Birukova, A. A., S. Chatchavalvanich, A. Rios, K. Kawkitinarong, J. G. N. Garcia, and K. G. Birukov. Differential regulation of pulmonary endothelial monolayer integrity by varying degrees of cyclic stretch. *Am. J. Pathol.* 168:1749–1761, 2006.
[4]Birukova, A. A., A. Rios, and K. G. Birukov. Long-term cyclic stretch controls pulmonary endothelial permeability at translational and post-translational levels. *Exp. Cell Res.* 314:3466–3477, 2008.
[5]Birukova, A. A., X. Tian, I. Cokic, Y. Beckham, M. L. Gardel, and K. G. Birukov. Endothelial barrier disruption and recovery is controlled by substrate stiffness. *Microvasc. Res.* 87:50–57, 2013.
[6]Brown, M. B., and A. B. Forsythe. 372: the ANOVA and multiple comparisons for data with heterogeneous variances. *Biometrics* 30:719–724, 1974.
[7]Casares, L., R. Vincent, D. Zalvidea, N. Campillo, D. Navajas, M. Arroyo, and X. Trepat. Hydraulic fracture during epithelial stretching. *Nat. Mater.* 14:343–351, 2015.
[8]Dudek, S. M., and J. G. N. Garcia. Cytoskeletal regulation of pulmonary vascular permeability. *J. Appl. Physiol.* 91:1487–1500, 2001.
[9]Hahn, C., and M. A. Schwartz. Mechanotransduction in vascular physiology and atherogenesis. *Nat. Rev. Mol. Cell Biol.* 10:53–62, 2009.
[10]Huang, L., P. S. Mathieu, and B. P. Helmke. A stretching device for high-resolution live-cell imaging. *Ann. Biomed. Eng.* 38:1728–1740, 2010.
[11]Huveneers, S., J. Oldenburg, E. Spanjaard, G. van der Krogt, I. Grigoriev, A. Akhmanova, H. Rehmann, and J. de Rooij. Vinculin associates with endothelial VE-cadherin junctions to control force-dependent remodeling. *J. Cell Biol.* 196:641–652, 2012.
[12]Huynh, J., N. Nishimura, K. Rana, J. M. Peloquin, J. P. Califano, C. R. Montague, M. R. King, C. B. Schaffer, and C. A. Reinhart-King. Age-related intimal stiffening enhances endothelial permeability and leukocyte transmigration. *Sci. Transl. Med.* 3:112ra122, 2011.
[13]Krishnan, R., D. D. Klumpers, C. Y. Park, K. Rajendran, X. Trepat, J. van Bezu, V. W. M. van Hinsbergh, C. V. Carman, J. D. Brain, J. J. Fredberg, J. P. Butler, and G. P. van Nieuw. Amerongen. Substrate stiffening promotes endothelial monolayer disruption through enhanced physical forces. *Am. J. Physiol. Cell Physiol.* 300:C146–C154, 2010.
[14]Li, L.-F., S.-K. Liao, C.-C. Huang, M.-J. Hung, and D. A. Quinn. Serine/threonine kinase-protein kinase B and extracellular signal-regulated kinase regulate ventilator-induced pulmonary fibrosis after bleomycin-induced acute lung injury: a prospective, controlled animal experiment. *Crit. Care* 12:R103, 2008.
[15]Liu, F., J. D. Mih, B. S. Shea, A. T. Kho, A. S. Sharif, A. M. Tager, and D. J. Tschumperlin. Feedback amplification of fibrosis through matrix stiffening and COX-2 suppression. *J. Cell Biol.* 190:693–706, 2010.
[16]Liu, W. F., C. M. Nelson, J. L. Tan, and C. S. Chen. Cadherins, RhoA, and Rac1 are differentially required for stretch-mediated proliferation in endothelial versus smooth muscle cells. *Circ. Res.* 101:e44–e52, 2007.
[17]Mammoto, A., T. Mammoto, M. Kanapathipillai, C. Wing Yung, E. Jiang, A. Jiang, K. Lofgren, E. P. S. Gee, and D. E. Ingber. Control of lung vascular permeability and

endotoxin-induced pulmonary oedema by changes in extracellular matrix mechanics. *Nat. Commun.* 4:1759, 2013.

[18]Maruthamuthu, V., B. Sabass, U. S. Schwarz, and M. L. Gardel. Cell-ECM traction force modulates endogenous tension at cell–cell contacts. *Proc. Natl. Acad. Sci. USA* 108:4708–4713, 2011.

[19]Ooi, C. Y., Z. Wang, D. M. Tabima, J. C. Eickhoff, and N. C. Chesler. The role of collagen in extralobar pulmonary artery stiffening in response to hypoxia-induced pulmonary hypertension. *Am. J. Physiol. Heart Circ. Physiol.* 299:H1823–H1831, 2010.

[20]Palchesko, R. N., L. Zhang, Y. Sun, and A. W. Feinberg. Development of polydimethylsiloxane substrates with tunable elastic modulus to study cell mechanobiology in muscle and nerve. *PLoS One* 7:e51499, 2012.

[21]Pelham, R. J., and Y.-L. Wang. Cell locomotion and focal adhesions are regulated by substrate flexibility. *Proc. Natl. Acad. Sci. USA* 94:13661–13665, 1997.

[22]Schaffer, J. L., M. Rizen, G. J. L'Italien, A. Benbrahim, J. Megerman, L. C. Gerstenfeld, and M. L. Gray. Device for the application of a dynamic biaxially uniform and isotropic strain to a flexible cell culture membrane. *J. Orthop. Res.* 12:709–719, 1994.

[23]Simmons, C. S., A. J. S. Ribeiro, and B. L. Pruitt. Formation of composite polyacrylamide and silicone substrates for independent control of stiffness and strain. *Lab Chip* 13:646–649, 2013.

[24]Spierenburg, G. T., F. T. J. J. Oerlemans, J. P. R. M. van Laarhoven, and C. H. M. M. de Bruyn. Phototoxicity of N-2-Hydroxyethylpiperazine-N′-2-ethanesulfonic acid-buffered culture media for human leukemic cell lines. *Cancer Res.* 44:2253–2254, 1984.

[25]Throm Quinlan, A. M., L. N. Sierad, A. K. Capulli, L. E. Firstenberg, and K. L. Billiar. Combining dynamic stretch and tunable stiffness to probe cell mechanobiology in vitro. *PLoS One* 6:e23272, 2011.

[26]Tschumperlin, D. J., and S. S. Margulies. Equibiaxial deformation-induced injury of alveolar epithelial cells *in vitro*. *Am. J. Physiol. Lung Cell. Mol. Physiol.* 275:L1173–L1183, 1998.

[27]Ungvari, Z., G. Kaley, R. de Cabo, W. E. Sonntag, and A. Csiszar. Mechanisms of vascular aging: new perspectives. *J. Gerontol. A-Biol.* 65A:1028–1041, 2010.

[28]Wang, Y., H.-H. Lai, M. Bachman, C. E. Sims, G. P. Li, and N. L. Allbritton. Covalent micropatterning of poly(dimethylsiloxane) by photografting through a mask. *Anal. Chem.* 77:7539–7546, 2005.